Progress Report for Year 2 of the Grant Titled: Boundary Conditions of the Heliosphere

Priscilla C. Frisch, P.I.
Jonathan D. Slavin
Eureka Scientific, Inc.

The following draft details the progress made in the work outlined in the grant proposal. We expect to submit this paper to the Astrophysical Journal within the next two months.

To be submitted to the Astrophysical Journal

The Ionization of the Local Interstellar Cloud

Jonathan D. Slavin[1]

Eureka Scientific Inc., 2452 Delmer St. Suite 100, Oakland, CA 94602-3017

and

Priscilla C. Frisch

University of Chicago, Department of Astronomy and Astrophysics, 5460 S. Ellis Avenue, Chicago, IL 60637

ABSTRACT

We present new calculations of the ionization of the Local Interstellar Cloud (LIC) by directly observed sources including nearby stellar EUV sources and the diffuse emission of the Soft X-ray Background (SXRB). In addition, we model the important, unobserved EUV emission both from the hot gas responsible for the SXRB and from a possible evaporative boundary between the LIC and the hot gas. We show that these ionization sources can provide the necessary ionization and heating of the cloud to match observations. Including the radiation from the conductive boundary, while not required, does improve the agreement with observations of the temperature of the LIC. The ionization predicted in our models shows good agreement with pickup ion results, interstellar absorption line data towards ϵ CMa, and EUV opacity measurements of nearby white dwarf stars. The areas of disagreement point to a possible underabundance (relative to solar abundance) of neon in the LIC. The presence of dust in the cloud, or at least depleted abundances, is necessary to maintain the heating/cooling balance and reach the observed temperature.

1. Introduction

The discovery of solar Lyα radiation fluorescing off of neutral interstellar hydrogen in the solar system proved that the Sun is immersed in a low density partially neutral interstellar cloud. Extreme ultraviolet (EUV) observations of the backscattered He^{o} 584Å line provided additional insight into the velocity and temperature of the interstellar gas observed within the the solar system.

---

[1]Also: Harvard-Smithsonian Center for Astrophysics, 60 Garden Street, MS 34, Cambridge, MA 02138

The overall characteristics of nearby interstellar material were determined by the *Copernicus* and IUE satellites. *Copernicus* data confirmed that the velocity of the gas producing the interplanetary Lyman α and He^{o} 584Å glow and the velocity of nearby interstellar material are similar. *Copernicus*, IUE and HST observations of nearby stars revealed that space densities in local interstellar matter (ISM) are relatively low (~ 0.1 cm^{-3}), that the gas is relatively warm (~ 7000 K) and that gas-phase abundances of refractory elements are enhanced relative to cold cloud abundances, indicating shock front destruction of dust grains. In addition, several interstellar clouds (i.e. absorption line velocity components) have been found within two parsecs of the Sun.

The very low column density of the interstellar cloud surrounding the solar system (the "local interstellar cloud," or LIC), and the cloud's location in the interior of the Local Bubble, allows the penetration of energetic photons to the interior of the LIC so that both helium and hydrogen are partially ionized. The ionization of nearby interstellar matter has been inferred from data on Mg^{o} /Mg^{+} , the fine-structure excited states C^{+*} , and observations of H^{o} and He^{o} towards nearby white dwarf stars. The discovery of the pickup ion (PUI) and anomalous cosmic ray (ACR) populations introduced a new possibility for determining the ionization of the LIC. Both PUIs and ACRs are believed to have as their source inflowing interstellar neutrals that are ionized in the Solar System.

The very local ISM may reveal important clues for understanding the ISM in general since the temperature and density of the LIC are similar to that of the warm ionized medium (WIM). The WIM is a major constituent of the interstellar medium, taking up $\gtrsim 20\%$ of its volume and as much as 1/3 of its mass. Most of our knowledge of the state of the WIM comes from observations of diffuse Hα emission, diffuse emission from other optical lines including [S II] λ6717, [N II] λ6584, [O III] λ5007, and [O I] λ6300, and pulsar dipersion measures. These observations all involve integrations over long pathlengths and therefore smooth out local variations in WIM properties. The ionization of the WIM inferred from such observations is considerably different from the LIC. [O I]λ6300Å observations have been used to infer that the WIM (in the limited regions for which the line has been observed) is highly ionized, $X_{\rm H} > 0.67$ (Reynolds 1989). In addition, observations of He I λ5876Å have been used to infer that helium is substantially *l*ess ionized than hydrogen in the WIM, $X_{\rm He} \lesssim 0.27 X_{\rm H}$ (Reynolds & Tufte 1995), though again the observations have been limited to a few locations near the galactic plane. For these reasons it is not clear if the LIC is representative of the WIM. The LIC represents one of the lowest column density interstellar clouds that has been detected in the disk, and such a cloud cannot be individually resolved in studies of more distant WIM gas. If the WIM is made up of a collection of ionized regions with a range of ionization characteristics, the LIC may represent the low ionization, hard ionization source end of that spectrum. Indeed, the LIC could be characteristic of warm, ionized clouds in regions with little to no O star radiation that are ionized primarily by radiation from hot gas (see below).

Alternatively, Welty et al. have shown that interstellar "clouds" typically represent blends of unresolved velocity components, with distinct properties. "Clouds" such as the interstellar cloud surrounding the solar system cannot be uniquely distinguished in blended sightlines, and are only observable in sightlines towards the nearest stars, or where high cloud velocities resolve weak

individual components (e.g. Spitzer). Therefore, the interstellar cloud surrounding the solar system represents a unique opportunity to determine the physics of a single interstellar cloud, including both gas and dust components, and to make in situ observations of that cloud.

There is no single, clearly dominant source for the ionization of the LIC. The directly observed sources of ionizing radiation fall into two categories: stellar EUV sources and diffuse soft x-ray background emission (SXRB). The former have all been observed by *EUVE* and the combined spectrum from the brightest sources has been presented by Vallerga (1998). The spectrum is unexpectedly dominated by the two B stars, ϵ CMa and β CMa. The most important part of the SXRB for ionization of the LIC is the low energy Be ($\sim$ 100 eV) and B band ($\sim$ 175 eV) radiation which has been been observed by the Wisconsin Group using rocket borne proportional counters.

Vallerga (1998) has shown that the stellar EUV sources are not capable of providing the observed He ionization. We show below that including the flux from the SXRB, modeled as emission from a 10^6 K collisional ionization equilibrium plasma, we can account for the observed ionization. We also show that better agreement with the observations can be achieved if we include the radiation from a evaporative interface at the boundary of the cloud.

Slavin (1989, hereafter S89) explored ionization of the Local Cloud due to ionizing radiation from the boundary of the cloud. In S89 the detailed temperature-density-ionization profiles at the interface of the cloud and the hot gas of the Local Bubble were calculated assuming that conduction was more or less inhibited by the magnetic field. We have improved on the calculations in S89 in several ways. First we treat the radiative transfer in the cloud much more carefully, utilizing the code CLOUDY (Ferland 1996) for this purpose. In addition we use improved atomic data and codes in our calculations of the radiation generated in the boundary and the resultant ionization. Moreover, substantial progress has been made in determining the physical state of the cloud in recent years and the differences in physical parameters from those assumed in S89 make a substantial difference in the ionization calculations.

2. The Local Interstellar Cloud and Its Environment

2.1. Local Cloud Properties

2.1.1. Density, Temperature and Magnetic Field

Perhaps the area in which the most progress has been made in determining the properties of the LIC is the temperature and density at the Solar System. Using direct detections by *Ulysses* the density of He^o has been found to be $n(\mathrm{He\ I}) = 0.017\ \mathrm{cm}^{-3}$. From these same observations the temperature is found to be $T = 6100 \pm 300$ K. Temperatures determined by observations of He I backscattered radiation, $T = 6900 \pm 600$ K (Flynn et al. 1998), is consistent with this result.

Line of sight data, i.e. ion column densities, derived from observations towards nearby stars

provide further constraints on our models of the ionization of the LIC. We compare our model results with observations of ϵ CMa below. Even over such a short sight line as through the LIC, however, the ionization, density and temperature are expected to vary significantly. Thus the *in situ* data provide extremely valuable constraints on our models that are unavailable for any other cloud in the ISM.

In contrast to the increasingly tight constraints on the temperature and density of the LIC, the magnetic field strength in the cloud remains poorly determined. While extremely high fields ($\gtrsim 8\mu$G) appear increasingly unlikely due to the lack of detection of the heliospheric bow shock, the range of plausible values for the field still extends from $\sim$ 1 - 5μG. An argument in favor of the higher end of this range is that the pressure support provided by a field of this strength would help support it against the apparently high thermal pressure of the Local Hot Bubble. Estimates of the bubble pressure based on the observed soft X-ray emission put it at $P/k \sim 10^4$ cm^{-3} K. The thermal pressure in our cloud models is more than a third less than that. Nevertheless, the pressure determination for the Local Bubble is indirect and subject to several uncertainties. As a result we explore models with $B = 2\mu$G and 5μG to span the range of likely values.

2.1.2. Dust content and Elemental Abundances

The gas phase elemental abundances in the LIC are of critical importance in determining the cooling rate of the gas. In addition, the fraction of the abundant elements that are tied up in dust can provide us with important information on the nature of the dust in the LIC and, by extension, in the WIM in general. Interstellar dust from the LIC has been directly observed by detectors on both the *Ulysses* and *Galileo* satellites. The dust size distribution and dust-to-gas ratios determined from those observations are problematic for current dust models as discussed in detail in Frisch et al. (1999). We have found that the actual dust content of the cloud is not of great importance for the heating/cooling balance since dust photoelectric heating is a minor contributor ($\sim 2\%$) to the total heating rate. The abundances of C, N, O and Fe on the other hand, control the cooling rate and thus the thermal balance in the LIC.

The gas phase abundances of these important elements is not simple to determine from observations. The primary difficulty in inferring the abundances is the uncertainty in the ionization correction in the LIC. Unlike many situations in the ISM, the LIC is neither nearly completely ionized nor completely neutral, but is partially ionized with a significant gradient in the ionization of the cloud from center to edge. Most importantly we do not have any direct measurement of the degree of ionization of hydrogen, though we have some rough limits. Because of these uncertainties, we treat the gas phase abundances of C, N, O, Mg, Si and Fe as parameters to be fixed in order to get agreement with observed column densities. Because of its proximity and the quality of the observational data, we use column densities towards ϵ CMa as determined by Gry & Dupin (1998) for this modeling. As we discuss in more detail below, we choose to fit our models to the column densities for the combined "LIC" and "Blue Cloud" (BC) components observed towards ϵ CMa. We adjust

the abundances in our model so that our calculated column densities of N(C II), N(N I), N(O I), N(Mg II), N(Si II)and N(Fe II)match the observed column densities. The abundances necessary to achieve agreement with the observations can then be seen as the model result and compared with our expectations for elemental depletions and undepleted ("reference") abundances.

2.2. The Local Interstellar Ionizing Radiation Field

The local interstellar radiation field (ISRF) is the primary input to any model for the ionization of the LIC. The degree of uncertainty in the intensity of the field varies greatly over the energy range of importance for the ionization of the cloud ($\sim 8 - 100$ eV). Although still quite uncertain, perhaps the best determined part of the spectrum is the far UV that comes primarily from B stars. In our models we have used the FUV fields of Mathis et al. (1983) and Gondhalekar et al. (1980). The diffuse soft x-ray background is also very important to the ionization of the cloud and has been observed over the entire sky by the Wisconsin Group (McCammon et al. 1983) and with *ROSAT* (Snowden et al. 1997). The limited energy resolution of the soft x-ray observations does not allow tight constraints to be put emission source, though thermal emission from a hot plasma appears most likely. The different instruments that have observed the soft x-ray diffuse background have found consistent results for the flux in the various energy bands covering energy ranges from ~ 120 eV to 1 keV and beyond. Thus by using the broad band count rates to fix the intensity (i.e. the emission measure, see below) in our model radiation field we have some confidence that the photoionization rates due to soft x-rays are fairly accurate. Since the radiation from an optically thin hot plasma is expected to be dominated by line emission, however, we need to keep in mind that a coincidence of an emission line and an absorption edge can still cause substantial differences in photoionization rates for spectra that produce the same band rates. Of much more importance, however, is the extrapolation of the emission spectrum to lower energies, i.e. the EUV (13.6 - 100 eV) which dominates the ionization of all of the elements with first ionization potential of 13.6 eV and higher.

The radiation field at EUV energies has at least two distinct components: stellar flux from white dwarfs and early type stars, and diffuse emission from the plasma of the Local Bubble. Observations carried out with *EUVE* have determined flux from all of the brightest stellar EUV sources (Vallerga 1998). The stellar flux is dominated by emission from two B stars, ϵ CMa and β CMa. The diffuse EUV emission has been searched for but has not been clearly detected to date (see, e.g. Vallerga & Slavin 1998), though the observation is difficult and no instrument optimized for observations of diffuse emission in the EUV has yet been flown. In this paper we take the simple approach of using the soft x-ray observations to fix the parameters of the model (emission measure, $\int n_e n_{\rm H+}\, ds$, and temperature) and then use the emission calculated by the model at lower energies. We discuss some of the uncertainties inherant in this approach below. Another uncertain, yet possibly dominant, contributor to the ionizing radiation field in the EUV is emission generated in the boundary between the Local Cloud and the surrounding gas of the Local Bubble.

3. Modeling the Ionization

3.1. Radiation from an Evaporative Boundary

If the Local Bubble gas is hot, $T \approx 10^6$ K, as inferred from the soft x-ray background observations, then a sharp temperature gradient should exist at the boundary between that hot gas and the warm, $T \approx 7000$ K LIC gas. In such an interface thermal conduction should cause heat to flow into the cloud and drive an evaporative outflow resulting in mass loss from the cloud (see e.g. Cowie & McKee 1977). As an important side effect, the cloud gas that is being heated, ionized and accelerated outward should radiate strongly in the EUV.

We have created models of the evaporative boundary that are similar to those of S89. We assume steady flow evaporation and spherical symmetry and include the effects of radiative cooling, non-equilibrium ionization and saturation of heat flux. The spectra (as well as necessary ionization, recombination and cooling rates) are calculated using the Raymond & Smith plasma emission code (Raymond & Smith 1977, and updates).

The parameters that need to be specified for the models include the cloud density, n_{cl} (total density including H and He), cloud radius, R_{cl}, temperature of the hot gas (i.e. at some large r from the center of the cloud – we choose 30 pc), T_h and cloud magnetic field strength, B_0. In addition we specify a conductivity reduction factor, η, which reduces the thermal conductivity of the gas in the way that would occur if the mean field direction were at some angle θ relative to the temperature gradient, where $\eta = \cos^2(\theta)$. We have chosen to always set $\eta = 0.5$ which is the mean value for a field that could be at any random angle to the radial direction. Note that this is different than assuming a randomly tangled field which would result in sharply reduced conductivty. The ionizing radiation field also affects the cloud evaporation due to the effect of ionization, particularly of H and He, on the total radiative cooling within the outflow. [In steady flow, the heat flowing into the cloud via thermal conduction is balanced by the radiative cooling in the interface and the enthalpy flowing out of the cloud.] Thus we need to specify parameters that influence the radiation field such as the total H I column density and the abundances of the most important elements.

In all the models presented we have used $R_{cl} = 3\,\mathrm{pc}$ and $\eta = 0.5$. We have done runs with $n_{cl} = 0.3$, 0.33 and 0.35; $B_0 = 2$ and $5\,\mu$G and $T_h = 10^6$ and $10^{6.1}$ K. In addition, we have looked at the effects of varying the cloud column density, $N_{\rm HI}$. This is allowed because, while the total column density towards nearby stars is determined by the *EUVE* observations, the column density between the sun and the edge of the LIC is not. That is, the *EUVE* lines of sight could be, and in many cases surely are, sampling more distant clouds in addition to the LIC. We have done runs for $N_{\rm HI} = 4 \times 10^{17}$, 6.5×10^{17} and $9 \times 10^{17}\,\mathrm{cm}^{-2}$. Our choice of $N_{\rm HI}$ affects the degree to which the hot gas and interface emission is absorbed between the edge of the LIC and the Sun but does not affect the stellar EUV emission. This is because we start with the observed flux and "de-absorb" by the amount appropriate to our assumed column density for the LIC to get the flux incident on the cloud face. The parameter values for each model run are listed in table 1.

3.2. The Combined Radiation Field and Radiative Transfer

To construct the total radiation field then, we take the cloud boundary spectrum we have generated and combine it with the stellar EUV spectrum and additional soft x-ray emission from hot gas. The emission from the hot gas is generated under the assumption of collisional ionization equilibrium of an optically thin plasma using the Raymond & Smith (1977, plus updates) plasma emission code. The total soft x-ray emission (including both the cloud boundary emission and diffuse emission from the Local Bubble) is scaled so as to give us the observed count rate in the Wisconsin B band ($\sim$ 180 eV). We choose to peg our flux to these observations since the B band is the softest x-ray band for which there are observations that cover the entire sky. We have also examined cases in which we assume no evaporation of the LIC so that all the soft x-ray emission comes from the hot gas of the Local Bubble. As we discuss below, our results for the ionization provide a worse match to the observations for these cases. We show in Figure 1 an example of a radiation field constucted for one of our models (no. 18, our preferred model discussed below).

To calculate the ionization in the cloud we employ the radiative transfer/thermal equilibrium code CLOUDY (Ferland 1996). CLOUDY calculates the detailed radiative transfer, including absorption and scattering, of the incident field and the diffuse continuum and emission lines generated within the cloud. The thermal and ionization balance is calculated at each point within the cloud.

4. Model Results

4.1. Column Densities and Abundances

In order to constrain our models and to derive information on the gas phase elemental abundances in the LIC we have chosen to tie our models to observations of several ion column densities towards ϵ CMa (Gry & Dupin 1998). As mentioned above, we choose to use the combined LIC and BC column densities to compare to. This assumption is discussed in more detail below.

Table 3 shows our results for the column densities predicted by our models. The column densities used as inputs to the model, N(C II), N(N I), N(O I), N(Mg II), N(Si II)and N(Fe II), are not listed since those are matched by adjusting the abundances. The observed values for those column densities, along with other observed quantities that we attempt to match, are listed in Table 2. Among the observations that we can directly compare to are observations of the column density ratios N(Mg II)/N(Mg I), N(C II)/N(C II*)and N(H I)/N(He I).

The first of these, N(Mg II)/N(Mg I), is a good indicator of electron density, yet it has some dependence on the strength of the FUV field as well since that is what determines the ionization balance of Mg. Because the fraction of Mg that is neutral, $X(\mathrm{Mg}^0)$, is always quite small, even small (absolute) changes in $X(\mathrm{Mg}^0)$ can alter the ratio $X(\mathrm{Mg}^+)/X(\mathrm{Mg}^0)$ substantially. For this reason we have explored two different FUV fields, that of Mathis et al. (1983) and Gondhalekar et al. (1980). The FUV background of Gondhalekar et al. (1980) was based on direct observations

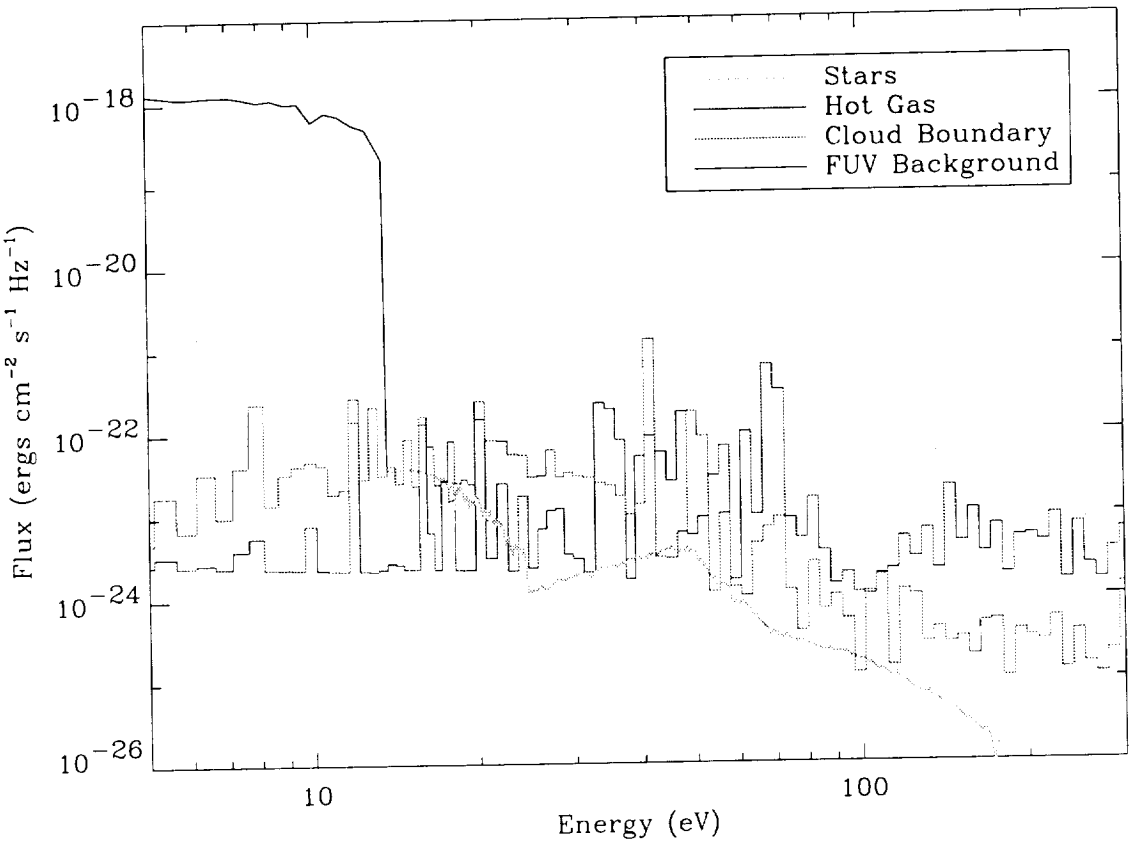

Fig. 1.— Model for the interstellar radiation field incident on the Local Cloud complex (model no. 18). The FUV part is mostly from B stars (Gondhalekar et al. 1980). The curve labeled "Stars" is the EUV flux from nearby stars (WD's and B stars) observed by *EUVE* (Vallerga 1998), deabsorbed by an H I column density of 4×10^{17} cm^{-2} so as to get the flux incident from outside the cloud. The "Cloud Boundary" curve is the flux from an evaporative interface between the cloud and the hot gas of the Local Bubble. The "Hot Gas" part of the background is due to the $\log T = 6.1$ gas in the Local Bubble with the intensity scaled so that the hot gas + interface radiation is consistent with the all-sky average count rate in the soft x-rays measured in the Wisconsin B band (McCammon et al. 1983).

of the radiation field with an extrapolation down to 912Å done by theoretical calculations of stellar emission and dust scattering and absorption. The intent of Mathis et al. (1983) was to describe the FUV field in a more general way that would apply to the Galaxy at different galactic radii. The differences in the two model backgrounds are not great (with the Mathis et al. (1983) flux somewhat larger than that of Gondhalekar et al. (1980)), yet they are large enough to affect the calculated N(Mg II)/N(Mg I)ratio in our models. As can be seen from comparison of the values of N(Mg II)/N(Mg I) in Table 3 with Table 2, in most cases the calculated ratio is larger than the observed ratio. This leads us to favor a lower FUV background flux, closer to that of Gondhalekar et al. (1980).

A more unambiguous indicator of electron density is the ratio N(C II)/N(C II*). In this case the only dependence besides the electron density is the weak dependence on temperature of the population of the excited fine structure ($J = 3/2$) level of the ground state of C^+, which only goes as $\sim T^{0.2}$ for $T \approx 7000$ K (Blum & Pradhan 1992). Moreover the temperature of the cloud is relatively well established as discussed above. It is these facts combined with the low observed value for N(C II)/N(C II*) that leads us to claim a higher electron density for the Local Cloud complex than has been claimed by some other investigators using different techniques. We find, as has Gry & Dupin (1998) directly from her observations, that we need an electron density of $n_e \approx 0.1$ in order to account for the N(C II)/N(C II*) ratio. This is achieved for certain of our models. though interestingly not for the models with no evaporative interface (nos. 19–25). It is the match with the observed N(C II)/N(C II*) ratio along with the temperature and n_{He^0} match that cause us to choose our model 18 as the "best-fit" model.

The column density of N(Ar I) is particularly interesting in that the ionization of Ar is a good discriminant between photoionization equilibrium models and non-equilibrium models in which the local cloud shows the signature of an earlier higher ionization state (Sofia & Jenkins 1998). As Sofia & Jenkins (1998) show, if the Local Cloud had been highly ionized at some earlier epoch, e.g. by a strong shock, and is in the process of recombining, then Ar I will be roughly equally ionized as H I since the recombination coefficients to for both ions are nearly the same. The photoionization cross section for Ar I, on the other hand is substantially larger than for H I, so if the ionization is due to the photoionizing background, then Ar I should be deficient. Jenkins et al. (2000) find, for lines of sight that include other gas in addition to the Local Cloud complex [check this], a low N(Ar I)/N(H I) ratio, favoring the photoionization equilibrium model over the fossil ionization picture. Our results show a range of values for N(Ar I)/N(H I) though generally showing an even greater ionization of Ar I than inferred by Jenkins et al. (2000). This could be due to the larger H I column densities observed (log N(H I)= 18.36 - 18.93), which indicates that some of the gas observed is not associated with the LIC [check this – note that we assume an abundance for Ar that is a factor of 1.12 lower than Jenkins et al (they use 3.31 ppm)].

The N(H I)/N(He I)ratio observed towards nearby stars has been one of the more difficult column density ratios to understand. If stellar sources, even very hot stars, are the dominant contributors to the interstellar radiation field, one expects H to be substantially more ionized than

He. If He has a 10% abundance, however, the mean observed value of 14 (Dupuis et al. 1995) indicates that He is significantly *more* ionized than H. Photoionization equilibrium thus demands a rather hard spectrum, dominated by diffuse EUV and soft x-ray emission with $E > 24.6$ eV. As can be seen from Table 3 some of our models do approach the observed average. These models are all ones with higher temperatures for the hot gas ($\log T_h = 6.1$) in accordance with the need for a relatively hard background spectrum. This result is consistent with the results of Snowden et al. (1998) who find the temperature of the emission from the Local Hot Bubble to be $\log T = 6.07 \pm 0.05$.

The gas phase elemental abundances of C, N, O, Mg, Si and Fe that we derive by combining our model results with the observations are listed in Table 5. Since different models have H I column densities that differ by as much as a factor of 2.25 (4×10^{17} cm^{-2}vs. 9×10^{17}), the abundances also vary by more than a factor of 2 between different models. Assuming a small value for N(H I) results in a high value for the abundances. There are some general features of our results, however. O and C have close to the same abundance with O up to 20% higher for some cases. This is in contrast to their solar abundance values (Grevesse 1984) which put the O abundance at ~66% higher than the C value. [mention B star values here] In addition, the values for C for the low N(H I) cases exceed the standard solar abundance value of 490 ppm. [Perhaps more discussion here of the "carbon crisis".] The derived abundance for O ranges from 31-70% below the solar value indicating depletion into dust. The abundance of N also slightly exceeds its solar value for the high N(H I) cases. Mg, Si and Fe (solar abundances 38, 35 and 47 ppm respectivley) on the other hand, are substantially depleted in all cases. Taken at face value, these results would indicate that graphite or other carbonaceous grains have been destroyed in the Local Cloud, but that silicate and iron grains have survived.

4.2. Densities, Ionization and Temperature at the Sun

Another important observational constraint on our models is the He^o density observed in interstellar gas flowing into the solar system. The observed value, n(He^o) = 0.017, is higher than would be expected if the electron density were low, $n_e < 0.1$. In addition, if the N(H I)/N(He I) column density ratio for the LIC+BC is close to the average value of 14 (Dupuis et al. 1995), then n(H^o) $\gtrsim$ 0.24, since the ionization of H will decrease into the cloud faster than that of He. The code we use to do the radiative transfer and thermal equilibrium, CLOUDY, uses the total (neutral + ionized) H density at the outer edge of the cloud as input. We find that we need initial densities of 0.3 cm^{-3} or more to match the observational constraints.

Our primary goal in this study is to determine the ionization state of the Local Cloud with a particular focus on the ionization near the position of the Solar System. Of particular importance is the ionization of H. We find that despite the large variation in a variety of parameters and other calculated quantities, the ionization fraction of H at the Sun varies relatively little between models, ranging from ~ 20% - 30%. The ionization of He ranges from ~ 30% - 50% in our models. Observations of anomolous cosmic rays (ACRs) and pickup ions (PUIs) in the Solar System provide

additional constraints on the ionization of the cloud. These comparisons are complicated in for some elements by the uncertain correction for "filtration" of interstellar neutrals that are ionized via charge exchange with solar wind ions at the heliopause. O and, to a much lesser degree N are expected to have lower fluxes in the Solar System due to this mechanism. Recent calculations by Izmodenov et al. (1997) put the filtration of O at 20-30%. From Table 4 we see that the model predictions for $n(O^0)/n(N^0)$ are close to the observed value, without correction for filtration. Thus if the filtration factor for O is 20% and that for N is very small, we predict too low a value for $n(O^0)/n(N^0)$. This can be seen as a direct consequence of pegging our model to the $N(O\ I)/N(N\ I)$ ratio oberved towards ϵ CMa, since the column density ratio and density ratio at the Sun is always close to the same (the ionization of O and N follow each other closely). We could be within the errors for $N(O\ I)$ and $N(N\ I)$ and obtain a higher ratio, ~ 10 and thus allow for 20% filtration of O. The calculated values of $n(O^0)/n(He^0)$ show much more variation from one model to the next. For our best fitting models, however, the calculated ratio is substantially above the observed value. In this case, applying a large filtration factor would help bring the calculated and observed ratios into agreement. The $n(N^0)/n(He^0)$ ratio again appears to be high compared with observations indicating that the problem with the model may have to do with overpredicting $n(N^0)$ which again would be helped by adopting a low value within the errors for $N(N\ I)$. Finally, the ratio $n(Ne^0)/n(He^0)$ is predicted to be much smaller than the observed value. We attribute this to assuming too small an elemental abundance of Ne. A substantially larger than "solar" value for the Ne abundance in the Local Cloud is thus a prediction of the model. In Figure 2 we plot the density of H I, He I, Ne I, O I and N I as a function of depth into the cloud for model 18, our "best fit" model. For almost all of the neutral ions, their density increases away from the cloud surface because the ionization level decreases. The degreee of variation of the densities indicaties the how much the position of the Sun within the cloud and the column density of the cloud can affect neutral ion density ratios derived from the PUI and ACR data.

The temperature of the Local Cloud turns out to be one of the more difficult observations to match. Many models that appear acceptable in other ways predict cloud temperatures that are substantially too high. As we discuss below, this could very well be due to errors and uncertainties in the atomic data used by the codes to calculate our models. Given the difficulties and uncertainties present in thermal equilibrium calculations, we consider it impressive that, without adjustment of parameters for this purpose, we are able to come so close to matching the temperature of the cloud at the Solar System.

5. Discussion

5.1. Model Assumptions and Reliability

There are a number of assumptions made in our modeling of the Local Cloud that may be questioned. Perhaps foremost of these is the assumption of steady state photoionization equilibrium

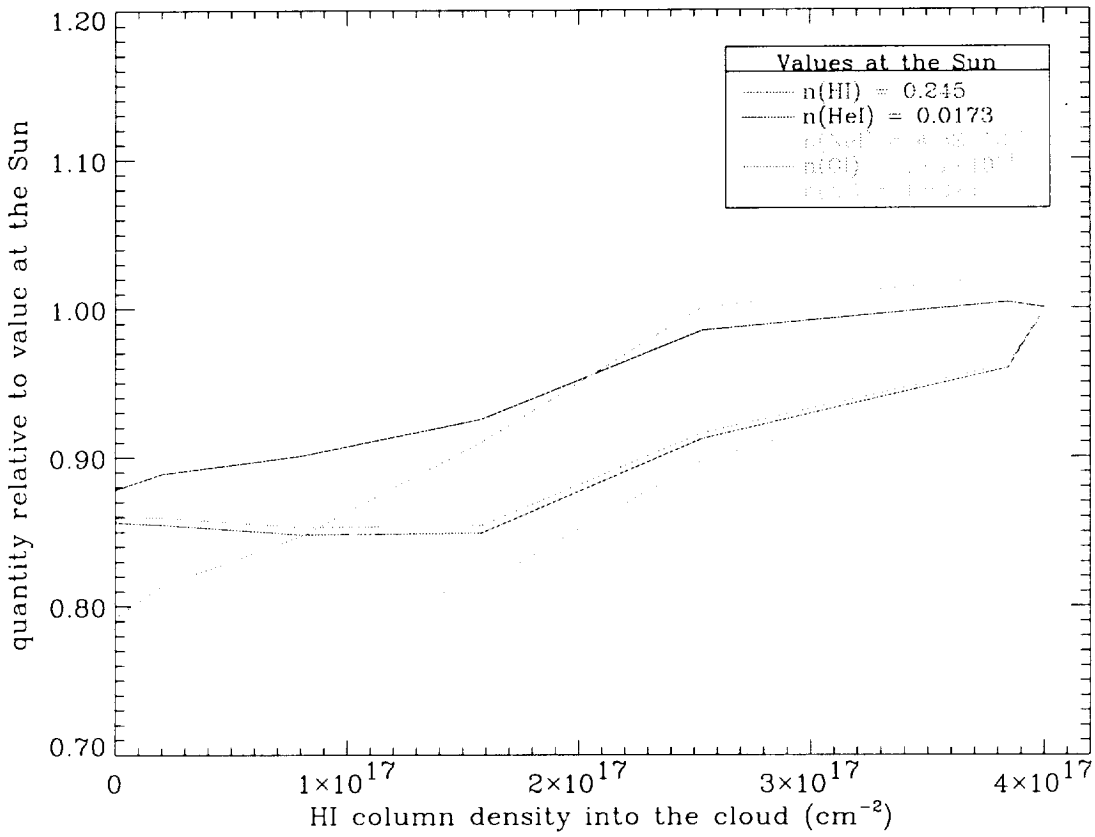

Fig. 2.— The densities of H I, He I, Ne I, O I, and N I relative to those at the Sun (for our model 18) as a function of depth (H I column density) into the cloud. The cloud surface is at the left and the solar location is at the right.

(see Lyu & Bruhweiler 1996). The H recombination time is $1/\alpha^{(2)} n_e \approx 9 \times 10^5$ yr, for $n_e = 0.1$ cm^{-3} and $T \approx 7000$ K and it is quite likely that the Local Cloud has experienced at least a moderately fast shock ($v_s \sim 50$ km s^{-1}) during that time. The observations of a low N(Ar I)/N(H I) by Jenkins et al. (2000) referred to above favor the interpretation that Ar is primarily photoionized and that non-equilibrium recombination is not the dominant effect in determining the ionization of Ar or H. We note in addition that our results show that the local insterstellar radiation field is quite capable of providing a moderately high level of ionization as is observed for the Local Cloud. Any fossil ionization from an energetic event (e.g. the passage of supernova shock) in the relatively recent past would appear to be insignificant at this point, since the ionization of the cloud does not seem to be in excess of what we expect from the ISRF.

One may also question the reliability and assumptions implicit in our calculations of the radiation field from the hot gas and the evaporative boundary. Plasma emission codes are currently in a state substantial revision and new and more detailed atomic data is being incorporated into these codes leading to significant changes in predicted spectra. The Raymond & Smith code that we have used to generate the background radiation field is known to be inaccurate in predicting a number of spectral features observed in recent x-ray spectra using, e.g. ASCA and the Chandra X-ray Observatory. These problems are of concern to us, though we feel, for the following reasons, that for our purposes the inaccuracies in the code probably do not strongly affect our results. First, we are concerned only with the photoionization caused by the background flux and not with the strength of individual line strengths. While individual spectral features could be incorrect, the cross section averaged flux may be fairly accurate. Second, we scale the field strength to be consistent with the observed band rate in the soft x-rays (i.e. the B band at ~ 100 eV), insuring that, at least over the range of the band coverage, the photon flux is not far from the true value. As more observations of the diffuse background, particularly in the EUV, and updated plasma emission codes become generally available, we will be able to revise our background spectrum and reevaluate the ionization rate in the LIC.

One particularly difficult aspect of the ionization calculation is the treatment of the geometry of radiative transfer. The sources of the background radiation field include: stars, point sources distributed across the sky (but dominated by ϵ CMa and β CMa); the hot gas of the Local Bubble, roughly evenly distributed across the sky and generated from the volume of the Bubble; and interface radiation generated in a thin volume between the warm gas of the cloud and the hot gas of the bubble. Each of these three sources demands a somewhat different radiative transfer technique. In addition the Sun is not at the center of the Local Cloud or the LIC/BC complex but rather appears to be near the edge. Moreover, the Blue Cloud seems to have a lower temperature and somewhat higher density than the LIC. Clearly the full radiative transfer calculation in this situation would be extremely difficult and subject to many uncertainties. Nevertheless, a more complex model may be warranted as more data on the shape and size of the Local Cloud and the background radiation fields becomes available since the ionization at the Solar System depends on somewhat sensitively on the ionizing flux recieved at our location within the cloud. In future work

we intend to refine our treatment of the radiative transfer in the cloud and explore its effects on the ionization at the solar location and throughout the cloud.

6. Summary

We have presented results of a calculation of the ionization of the Local Cloud complex (LIC and BC) due to the background interstellar radiation field. We have constructed the field from directly observed sources including nearby stellar sources (B stars and white dwarfs) and diffuse emission from the hot gas in the Local Hot Bubble. We have additionally included the emission from a proposed evaporative boundary between the warm cloud and surrounding hot gas. We find that this radiation field is capable of maintaining the ionization and heating necessary to explain a variety of observations including: column densities of several ions towards ϵ CMa neutral atom ratios derived from PUI data, the temperature of the cloud and the density of He I observed in the solar system.

We find that the high mean electron density as inferred from the ratio N(C II)/N(C II*) towards ϵ CMa requires a local electron density at the Sun, $n_e \approx 0.1$ cm^{-3}. This in turn requires a high EUV flux, larger than can be provided by either the stellar EUV flux or the diffuse emission from the hot gas of the Local Bubble. Thus we find evidence for an evaporative boundary to the Local Cloud as an additional source of EUV emission.

By tying our results to observed column densities for a number of ions towards ϵ CMa, we are able to draw conclusions on the gas phase elemental abundances of those elements. We find that the gas phase abundances of O, Mg, Si and Fe all show substantial depletion relative to solar abundances. N and especially C appear to be undepleted and even to have abundances somewhat above the standard solar vales. Taken at face value we would conclude that the LIC/BC complex has a significant amount of silicate and, possibly Fe dust but that the carbonaceous dust has been destroyed.

We also find that our models, which assume a gas phase abundance for Ne of 123 ppm, predict substantially lower values for the ratio $n(\mathrm{Ne}^0)/n(\mathrm{He}^0)$ than is observed in the PUIs. This suggests that Ne in the LIC could be significantly underabundant relative to solar abundances.

This research was supported by a NASA grant no. NASW-98027 of the "Earth-Sun Connection: Supporting Research and Technology" program. We have greatly benefitted from helpful discussions with Alan Cummings, George Gloeckler, Dick Mewaldt, and Gary Zank. PCF would also like to thank the Astronomy Department at the University of California, Berkeley, for acting as a host during part of this research.

REFERENCES

Blum, R. D. & Pradhan, A. K. 1992, ApJS, 80, 425

Cowie, L. L. & McKee, C. F. 1977, ApJ, 211, 135

Dupuis, J., Vennes, S., Bowyer, S., Pradhan, A. K., & Thejll, P. 1995, ApJ, 455, 574

Ferland, G. 1996, Hazy, a Brief Introduction to Cloudy (University of Kentucky Department of Physics and Astronomy Internal Report)

Flynn, B., Vallerga, J., Dalaudier, F., & Gladstone, G. R. 1998, J. Geophys. Res., 103, 6483

Frisch, P. C., Dorschner, J. M., Geiss, J., Greenberg, J. M., Grün, E., Landgraf, M., Hoppe, P., Jones, A. P., Krätschmer, W., Linde, T. J., Morfill, G. E., Reach, W., Slavin, J. D., Svestka, J., Witt, A. N., & Zank, G. P. 1999, ApJ, 525, 492

Gondhalekar, P. M., Phillips, A. P., & Wilson, R. 1980, A&A, 85, 272

Grevesse, N. 1984, Phys. Scr, 8, 49

Gry, C. & Dupin, O. 1998, in Berlin Springer Verlag Lecture Notes in Physics, v.506, Vol. 506, 161

Izmodenov, V., Malama, Y. G., & Lallement, R. 1997, A&A, 317, 193

Jenkins, E. B., Oegerle, W. R., Gry, C., Vallerga, J., Sembach, K. R., Shelton, R. L., Ferlet, R., Vidal-Madjar, A., York, D. G., Linsky, J. L., Roth, K. C., Dupree, A. K., & Edelstein, J. 2000, ApJ, 538, L81

Lyu, C. H. & Bruhweiler, F. C. 1996, ApJ, 459, 216

Mathis, J. S., Mezger, P. G., & Panagia, N. 1983, A&A, 128, 212

McCammon, D., Burrows, D. N., Sanders, W. T., & Kraushaar, W. L. 1983, ApJ, 269, 107

Raymond, J. C. & Smith, B. W. 1977, ApJS, 35, 419

Reynolds, R. J. 1989, ApJ, 345, 811

Reynolds, R. J. & Tufte, S. L. 1995, ApJ, 439, L17

Slavin, J. D. 1989, ApJ, 346, 718

Snowden, S. L., Egger, R., Finkbeiner, D. P., Freyberg, M. J., & Plucinsky, P. P. 1998, ApJ, 493, 715

Snowden, S. L., Egger, R., Freyberg, M. J., McCammon, D., Plucinsky, P. P., Sanders, W. T., Schmitt, J. H. M. M., Truemper, J., & Voges, W. 1997, ApJ, 485, 125

Sofia, U. J. & Jenkins, E. B. 1998, ApJ, 499, 951

Vallerga, J. 1998, ApJ, 497, 921

Vallerga, J. & Slavin, J. 1998, in Berlin Springer Verlag Lecture Notes in Physics, v.506, Vol. 506, 79

Witte, M., Banaszkiewicz, M., & Rosenbauer, H. 1996, Space Science Reviews, 78, 289

Table 1. Model Input Parameter Values

	Input Parameter Type				
Model No.	$n_{\rm H}$ (cm^{-3})	$\log T_h$	B_0 (μG)[a]	$N_{\rm HI}$ (10^{17} cm^{-2})	FUV field[b]
1	0.273	6.0	5.0	4.0	MMP
2	0.273	6.0	5.0	6.5	MMP
3	0.273	6.0	5.0	9.0	MMP
4	0.273	6.0	2.0	4.0	MMP
5	0.273	6.0	2.0	6.5	MMP
6	0.273	6.0	2.0	9.0	MMP
7	0.273	6.1	5.0	4.0	MMP
8	0.273	6.1	5.0	6.5	MMP
9	0.273	6.1	5.0	9.0	MMP
10	0.273	6.1	2.0	4.0	MMP
11	0.273	6.1	2.0	6.5	MMP
12	0.273	6.1	2.0	9.0	MMP
13	0.300	6.0	5.0	4.0	MMP
14	0.300	6.0	5.0	4.0	GPW
15	0.300	6.1	5.0	4.0	MMP
16	0.300	6.1	5.0	9.0	MMP
17	0.318	6.1	5.0	4.0	MMP
18	0.318	6.1	5.0	4.0	GPW
19	0.273	6.0	···	4.0	MMP
20	0.273	6.0	···	6.5	MMP
21	0.273	6.0	···	9.0	MMP
22	0.273	6.1	···	4.0	MMP
23	0.273	6.1	···	6.5	MMP
24	0.273	6.1	···	9.0	MMP
25	0.227	6.0	···	4.0	MMP

[a]models for which no magnetic field strength is given are those for which we have assumed that the cloud boundary is not conductive so that there is no evaporative interface

[b]Reference for FUV background field strength and shape. MMP is Mathis, Mezger & Panagia (1983) and GPW refers to Gondhalekar, Phillips & Wilson (1980).

Table 2. Observational Constraints

Observed Quantity	Observed Value	References[a]
N(C II) (cm^{-2})	$3.1 \pm 0.3 \times 10^{14}$	1
N(C II*) (cm^{-2})	$2.05 \pm 0.35 \times 10^{12}$	1
N(N I) (cm^{-2})	$2.60 \pm 0.10 \times 10^{13}$	1
N(O I) (cm^{-2})	$2.3 \pm 0.2 \times 10^{14}$	1
N(Mg I) (cm^{-2})	$1.3 \pm 0.35 \times 10^{10}$	1
N(Mg II) (cm^{-2})	$4.0 \pm 0.2 \times 10^{12}$	1
N(Si II) (cm^{-2})	$1.5 - 5.0 \times 10^{12}$	1
N(Si III) (cm^{-2})	$< 6.0 \times 10^{12}$	1
N(Fe II) (cm^{-2})	$1.87 \pm 0.10 \times 10^{12}$	1
N(H I)/N(He I)	14 ± 0.4[b]	2
n(O I)/n(N I)	8.1 ± 1.66	3
n(O I)/n(He I)	$5.2 \pm 0.1 \times 10^{-3}$	3
n(N I)/n(He I)	$6.4 \pm 1.3 \times 10^{-4}$	3
n(Ne I)/n(He I)	$1.1 \pm 0.18 \times 10^{-3}$	3
T(K)	6700 ± 900	4
n(He I) (cm^{-3})	0.017 ± 0.002	4

[a](1) Gry & Dupin (1998), (2) Dupuis et al. (1995), (3) Gloeckler, G., (2000) private communication, (4) Witte et al. (1996)

[b]The uncertainty given is only that due to uncertainties listed in Dupuis et al. (1995) for the observed H I and He I column densities with the implicit assumption that the ratio is the same on all lines of sight. The data indicate, however, that there is substantial intrinsic variation in this ratio and thus the quoted uncertainty must be regarded as a lower limit to the true uncertainty in the ratio.

Table 3. Model Column Density Results

Model	$\log N(\mathrm{H_{tot}})$	$\log N(\mathrm{Ar\ I})$	$\log N(\mathrm{Ar\ II})$	$\log N(\mathrm{Si\ II})$	$\log N(\mathrm{Si\ III})$	$\frac{N(\mathrm{Mg\ II})}{N(\mathrm{Mg\ I})}$	$\frac{N(\mathrm{C\ II})}{N(\mathrm{C\ II}^*)}$	$\frac{N(\mathrm{H\ I})}{N(\mathrm{He\ I})}$
1	17.80	11.45	11.96	13.10	10.54	497.6	183.4	12.37
2	18.03	11.71	12.19	13.09	10.75	364.0	182.0	11.63
3	18.19	11.93	12.37	13.10	10.85	333.7	168.5	10.16
4	17.74	11.55	11.91	13.09	10.17	816.6	219.4	12.15
5	17.98	11.81	12.15	13.10	10.50	518.4	211.4	11.17
6	18.16	12.02	12.35	13.10	10.66	442.4	184.3	9.55
7	17.79	11.42	11.93	13.09	10.64	416.2	185.8	13.59
8	18.02	11.69	12.17	13.10	10.81	323.9	185.0	12.74
9	18.20	11.90	12.36	13.10	10.92	298.4	168.2	10.93
10	17.75	11.52	11.90	13.10	10.35	622.7	221.8	13.02
11	17.99	11.78	12.14	13.10	10.62	427.0	210.5	11.93
12	18.17	11.99	12.34	13.09	10.75	377.8	183.1	10.03
13	17.79	11.46	11.95	13.10	10.47	505.1	171.1	12.29
14	17.79	11.46	11.95	13.10	10.47	444.0	170.9	12.29
15	17.78	11.44	11.93	13.09	10.58	419.4	174.0	13.45
16	18.19	11.92	12.35	13.10	10.88	293.9	157.7	10.92
17	17.78	11.45	11.93	13.10	10.55	422.3	167.0	13.36
18	17.78	11.45	11.93	13.10	10.55	372.1	166.9	13.36
19	17.70	11.64	11.87	13.09	9.56	1488	250.5	11.57
20	17.95	11.89	12.12	13.09	10.23	790.1	235.9	10.53
21	18.14	12.10	12.32	13.10	10.41	633.4	198.5	8.90
22	17.72	11.58	11.88	13.09	10.12	862.3	249.8	12.60
23	17.97	11.85	12.13	13.10	10.47	543.2	230.5	11.36
24	18.15	12.06	12.33	13.10	10.61	469.3	195.3	9.46
25	17.73	11.60	11.89	13.10	9.94	1283	284.1	11.76

Table 4. Model Results for Solar Location

Model	X(H)	X(He)	O I/N I	O I/He I	N I/He I	Ne I/He I	T	n(H I)	n(He I)	n_e
1	0.314	0.468	8.45	7.39×10^{-3}	8.75×10^{-4}	3.00×10^{-4}	7150	0.205	0.0156	0.107
2	0.285	0.470	8.82	4.77×10^{-3}	5.41×10^{-4}	2.87×10^{-4}	8150	0.209	0.0153	0.0977
3	0.235	0.444	8.76	3.50×10^{-3}	4.00×10^{-4}	2.95×10^{-4}	8430	0.237	0.0170	0.0878
4	0.232	0.400	8.69	7.43×10^{-3}	8.55×10^{-4}	3.41×10^{-4}	6460	0.234	0.0180	0.0827
5	0.221	0.408	8.80	4.73×10^{-3}	5.37×10^{-4}	3.17×10^{-4}	7760	0.225	0.0168	0.0756
6	0.205	0.391	8.96	3.31×10^{-3}	3.69×10^{-4}	3.17×10^{-4}	8190	0.232	0.0175	0.0721
7	0.305	0.512	8.42	8.26×10^{-3}	9.81×10^{-4}	2.41×10^{-4}	7640	0.203	0.0139	0.105
8	0.298	0.510	8.79	5.14×10^{-3}	5.85×10^{-4}	2.38×10^{-4}	8430	0.202	0.0137	0.101
9	0.274	0.487	8.99	3.66×10^{-3}	4.07×10^{-4}	2.43×10^{-4}	8700	0.215	0.0148	0.0966
10	0.251	0.436	8.66	7.81×10^{-3}	9.01×10^{-4}	2.75×10^{-4}	7010	0.221	0.0163	0.0885
11	0.255	0.442	8.78	4.75×10^{-3}	5.41×10^{-4}	2.63×10^{-4}	8090	0.212	0.0155	0.0864
12	0.216	0.425	8.82	3.49×10^{-3}	3.96×10^{-4}	2.62×10^{-4}	8470	0.228	0.0164	0.0766
13	0.306	0.455	8.52	7.27×10^{-3}	8.54×10^{-4}	3.14×10^{-4}	7000	0.228	0.0177	0.116
14	0.306	0.454	8.52	7.25×10^{-3}	8.52×10^{-4}	3.14×10^{-4}	7000	0.228	0.0178	0.116
15	0.293	0.497	8.63	8.30×10^{-3}	9.61×10^{-4}	2.53×10^{-4}	7490	0.229	0.0159	0.112
16	0.266	0.476	8.87	3.61×10^{-3}	4.07×10^{-4}	2.53×10^{-4}	8630	0.239	0.0166	0.102
17	0.287	0.486	8.53	8.18×10^{-3}	9.58×10^{-4}	2.61×10^{-4}	7380	0.245	0.0173	0.117
18	0.287	0.486	8.53	8.18×10^{-3}	9.58×10^{-4}	2.61×10^{-4}	7380	0.245	0.0173	0.117
19	0.177	0.330	8.89	7.09×10^{-3}	7.98×10^{-4}	3.95×10^{-4}	5490	0.254	0.0204	0.0653
20	0.186	0.349	8.97	4.47×10^{-3}	4.99×10^{-4}	3.46×10^{-4}	7340	0.226	0.0178	0.0615
21	0.188	0.319	9.20	3.01×10^{-3}	3.27×10^{-4}	3.56×10^{-4}	7790	0.226	0.0187	0.0616
22	0.204	0.396	8.67	7.70×10^{-3}	8.89×10^{-4}	2.90×10^{-4}	6660	0.235	0.0174	0.0725
23	0.227	0.395	9.01	4.63×10^{-3}	5.14×10^{-4}	2.79×10^{-4}	7830	0.216	0.0165	0.0751
24	0.213	0.373	9.18	3.21×10^{-3}	3.49×10^{-4}	2.82×10^{-4}	8240	0.220	0.0171	0.0710
25	0.209	0.359	8.76	7.17×10^{-3}	8.18×10^{-4}	3.62×10^{-4}	6040	0.201	0.0160	0.0624

Table 5. Elemental Gas Phase Abundances (ppm)

	Element					
Model No.	C	N	O	Mg	Si	Fe
1	513	79.4	550	7.59	20.0	3.16
2	302	47.9	339	4.47	11.7	1.86
3	204	33.9	245	3.02	8.13	1.29
4	575	72.4	562	8.71	22.4	3.47
5	331	45.7	347	5.01	13.2	2.04
6	219	31.6	245	3.24	8.71	1.35
7	513	83.2	550	7.94	20.0	3.16
8	309	50.1	339	4.68	12.0	1.86
9	204	34.7	245	3.09	7.94	1.26
10	575	75.9	562	8.91	22.4	3.47
11	331	46.8	339	5.25	12.9	2.00
12	219	33.1	245	3.39	8.51	1.35
13	525	77.6	550	7.59	20.4	3.16
14	525	77.6	550	7.59	20.4	3.16
15	525	81.3	562	8.13	20.4	3.24
16	209	34.7	245	3.16	8.13	1.29
17	537	81.3	562	8.13	20.9	3.24
18	537	81.3	562	8.13	20.9	3.24
19	617	66.1	562	9.55	24.5	3.80
20	355	42.7	347	5.37	13.8	2.14
21	229	29.5	245	3.47	9.12	1.41
22	603	72.4	562	9.77	23.4	3.63
23	347	44.7	347	5.50	13.5	2.09
24	224	30.9	245	3.47	8.91	1.38
25	589	69.2	562	9.33	23.4	3.63

REPORT DOCUMENTATION PAGE

Form Approved
OMB No. 0704-0188

1. AGENCY USE ONLY (Leave blank)	2. REPORT DATE	3. REPORT TYPE AND DATES COVERED
	4/1/01	Final 3/11/99-3/10/01

4. TITLE AND SUBTITLE

Boundary Conditions of the Heliosphere

5. FUNDING NUMBERS

NASW-98027

6. AUTHOR(S)

Dr. Priscilla Frisch & Jonathan Slavin

7. PERFORMING ORGANIZATION NAME(S) AND ADDRESS(ES)

Eureka Scientific, Inc
2452 Delmer St., Ste. 100,
Oakland, CA 94602

8. PERFORMING ORGANIZATION REPORT NUMBER

9. SPONSORING / MONITORING AGENCY NAME(S) AND ADDRESS(ES)

10. SPONSORING / MONITORING AGENCY REPORT NUMBER

11. SUPPLEMENTARY NOTES

12a. DISTRIBUTION / AVAILABILITY STATEMENT

12b. DISTRIBUTION CODE

13. ABSTRACT *(Maximum 200 words)*

Please See Attached

14. SUBJECT TERMS

15. NUMBER OF PAGES
22

16. PRICE CODE

17. SECURITY CLASSIFICATION OF REPORT	18. SECURITY CLASSIFICATION OF THIS PAGE	19. SECURITY CLASSIFICATION OF ABSTRACT	20. LIMITATION OF ABSTRACT